Applied Clay Science 276 (2025) 107901

Contents lists available at ScienceDirect

Applied Clay Science

journal homepage: www.elsevier.com/locate/clay

Research Paper

Mineralogical and geotechnical characterization of two German bentonites from Westerwald and Bavaria☆

A. Asaad [a,*], A. Nitsch [b], W. Baille [b], K. Emmerich [a]

[a] Institute of Concrete Structures and Building Materials (IMB/MPA/CMM), Karlsruhe Institute of Technology (KIT), Karlsruhe, Germany
[b] Chair of Soil Mechanics, Foundation Engineering and Environmental Geotechnics, Department of Civil and Environmental Engineering, Ruhr-University Bochum, Bochum, Germany

ARTICLE INFO

Keywords:
Bentonite
Radioactive waste
Mineralogy
Geotechnique
Smectite
Calcigel

ABSTRACT

This study investigates the fundamental mineralogical, physico-chemical, and geotechnical properties of two naturally occurring Ca/Mg bentonites from Germany, along with their Na-saturated sub-fractions. The bentonites — Secursol UHP® from Westerwald and Calcigel® from Bavaria — are commercially available and used in different forms, including granular and pillow types, for geotechnical purposes and multiscale testing of the Sandwich sealing system for hydraulic sealing in underground waste repositories. The dioctahedral smectite content in Secursol UHP and Calcigel is 79 % and 61 %, respectively. Smectite in both was identified as montmorillonitic beidellite with significant octahedral iron and no interstratification. Smectite in Secursol UHP shows a slightly higher layer charge and broader particle size distribution, while Calcigel smectite has a 25 % larger average basal surface and slightly greater stack thickness. Geotechnically, both are highly plastic clays with almost identical consistency as received; however, Calcigel exhibits a higher liquid limit, greater water uptake, and better dispersity in deionized water despite its lower smectite content, lower total specific surface area, and relatively coarser particles. These discrepancies are attributed to the inherited fabric of Secursol UHP hindering smectite expansion.

1. Introduction

In the 1970s, many countries initiated extensive research programs to develop safe geological repositories for high-level radioactive waste. Clay and clay-rich formations, due to their low hydraulic conductivity in a saturated state, were explored as potential host rocks to isolate radioactive waste from the surrounding biosphere for extremely long periods of time (Lee and Tank, 1985; Brennecke and Kunze, 2000; Landais, 2006; Sellin and Leupin, 2013; Delay et al., 2014; Bossart et al., 2017). In addition, compacted swelling clays, like bentonites, were investigated for the use in Engineered Barrier Systems (EBS), including buffer and backfill for waste canisters and sealing of shafts and drifts. Owing to their low hydraulic conductivity in a saturated state, swelling pressure, and ion retention capability (Allen and Wood, 1988; Pusch, 1992, 2006; Madsen, 1998; Emmerich et al., 2009a; Baille et al., 2010, 2016; Delage et al., 2010; Gruner, 2010; Asaad et al., 2021; Jalal et al., 2021; Liu et al., 2023).

A distinctive feature of German shaft seal designs is the Sandwich sealing system developed at the Karlsruhe Institute of Technology (KIT; Nüesch et al., 2002; Schuhmann et al., 2009). This system, in contrast to conventional monolithic bentonite seals, consists of alternating sealing segments (DS) made of compacted bentonite and equipotential segments (ES) composed of mineral material with higher hydraulic conductivity. The ES facilitate a homogeneous distribution of infiltrating fluid across the cross-section of the seal, thereby promoting uniform hydration and swelling of the bentonite in the DS. The Sandwich sealing system and its interaction with a potential host rock (i.e., Opalinus Clay) are currently being tested at large scale in an in-situ experiment at the international Mont Terri rock laboratory in Switzerland (Emmerich et al., 2019; Wieczorek et al., 2021;Wieczorek et al., 2024).

Long-term safety requirements for underground nuclear waste repositories demand specific properties in the bentonite used, such as a defined smectite content and a minimum swelling pressure. These requirements are often fulfilled by using technical bentonite blends, which are formulated to meet precise performance specifications. However, even when sourced from the same major supplier, the mineralogical,

☆ This article is part of a Special issue entitled: 'Clay Conf. Hannover 2024' published in Applied Clay Science.

* Corresponding author.
E-mail address: ali.asaad@kit.edu (A. Asaad).

https://doi.org/10.1016/j.clay.2025.107901
Received 25 January 2025; Received in revised form 6 June 2025; Accepted 7 June 2025
Available online 20 June 2025

Table 1
Average mineralogical composition of the Calcigel and Secursol UHP bentonites obtained from quantitative phase analysis performed on XRD patterns of random powder mounts.

		Secursol UHP				Calcigel			
		Literature	This work			Literature	This work		
			Raw	<2Na[a]	>2Na[a]		Raw	<2Na[a]	>2Na[a]
Smectite (di)		70.0–90.0	79.2	88.7	53.0	55.0–65.0	61.0	72.0	27.4
Kaolinite		1.0–5.0	2.5	2.9	1.6	2.0–4.0	2.1	1.7	1.0
Chlorite (tri)						1.0–2.0	1.3	1.6	1.4
Mica / Illite (di)		1.0–4.0	3.3	2.8	3.6	10.0–15.0	13.5	11.7	20.5
Quartz		2.0–10.0	10.7	1.5	35.5	8–15	16.0	12.0	47.3
Feldspars		1.0–6.0	0.8	0.8	1.7	1.0–3.0	1.0	0.5	1.7
Calcite	[wt%] room humidity					1.0–4.0	1.3	0.0	0.0
Dolomite						2.0–6.0	3.1	0.0	0.0
Anatase		1.0–3.0	2.2	3.1	2.7	0.0–1.0			
Rutile			0.1	0.1	0.1		0.7	0.5	0.7
Iron oxides (Hematite, Maghemite)		0.0–1.0	0.9	0.1	1.8				
Apatite		< 1.0	0.3						
Total			100.0	100.0	100.0		100.0	100.0	100.0
LC (AAM)	[eq./f.u.]		0.36				0.31		
a_s (N_2)	[m^2/g]		74.0	101.0	47.0		57.0	73.0	-[b]
a_s (EGME)	[m^2/g]		583.0				460.0		
Number of layers in stacks (*D*)				11.5	9.0			12.5	10.0

[a] < or > 2Na refer to the less or more than 2 μm Na-saturated size fraction.
[b] not enough material.

physico-chemical, and geotechnical properties of bentonite—as a natural material—can vary significantly between different mining and production batches. This variability has been demonstrated, for example, in the work of Dixon et al. (2023) on MX-80 bentonite and Asaad et al. (2022) on Illite du Puy.

Thorough mineralogical and geotechnical characterization of bentonite is essential for understanding its behavior in various applications and experimental setups, as well as for simulations assessing its long-term performance in underground repositories. Moreover, the availability of bentonite resources may be affected by political developments and economic decisions, potentially necessitating the replacement of a well-characterized bentonite with an alternative of similar properties but different origin and genesis. In Germany, four distinct sources of swelling clays are currently known (see Supplementary data). Although Bavarian bentonites, such as those marketed as Calcigel, have been studied for decades in geotechnical applications and EBS for deep geological repositories, significantly less data exist for other swelling clay deposits. Therefore, this study examines the mineralogical and geotechnical properties of two natural Ca/Mg bentonites—Calcigel from Bavaria and Secursol UHP from the Westerwald region and their suitability in the Sandwich sealing system. The aim is to establish a baseline of physico-chemical data for these commercially available materials, which are not only relevant for geotechnical applications but also widely used in various chemical and technical fields.

1.1. Materials

1.1.1. Raw material

Secursol UHP® and Calcigel® are the commercial names of Ca/Mg-bentonites from Germany. Secursol UHP is mined from three open pits (Arborn, Ruppach, and Salz) in Ruppach-Goldhausen (Westerwald region), and Calcigel from Moosburg area (Landshut region, Bavaria). Their mineralogical properties reported in the literature are summarized in Table 1 from (Madsen, 1998; Herbert and Moog, 2002; Hlug, 2006; Königer et al., 2008; Emmerich et al., 2009a, 2009b; Baille et al., 2010; Svensson et al., 2011; Steudel and Emmerich, 2013; Delavernhe et al., 2015; Bengtsson and Pedersen, 2017; Schanz et al., 2018; Trümer et al., 2019; Fontaine et al., 2020; Emmerich et al., 2021). In addition, the supplementary data of this work includes a comprehensive review of commercial bentonite deposits in Germany, comparing their mineralogical and geotechnical properties as reported in the literature.

Both bentonites were provided by the Stephan Schmidt Group (SSKG, Dornburg) as granular material (0–4 mm) obtained from crushing of compacted pillows (pellets) to be used in semi-technical scale experiments (HTV) and in in-situ experiments (i.e., Shaft 1 and Shaft 2) at Mont Terri rock laboratory (Wieczorek et al., 2024). Calcigel was dried to 10 % water content (105°C) and milled (< 500 μm) by the producer (Clariant). The provided powder was compacted into pillows, part is used in HTV 7 and Shaft 1, and another part was crushed into granules (<4 mm). Secursol UHP was dried after mining by SSKG to about 12 % water content (105°C) and crushed in a roller mill (< 3.5 mm) in two steps for pillows production. Part of these pillows were used in HTV 6 (Emmerich et al., 2019), and another part was crushed into granules (<4 mm) for the current study.

1.1.2. Pretreatment and size separation

300 g of granular material were dispersed in 3 L of a buffer solution of 2 M sodium acetate p.a. (CH_3COONa) and 2 M acetic acid (100 %) at a ratio of 2:1. The dispersion was stirred for 4–6 h, and left to coagulate. pH was maintained at approximately 4.8. After coagulation, the clear supernatant was removed, and replaced by fresh buffer solution. This process was repeated until no more gas bubbles, predominantly CO_2 from carbonates, were visible. Next, the material was washed with a 1 M NaCl solution (4×), then rinsed with deionized water to eliminate excess salt (centrifugation at 4500 rpm for 30 min, Heraeus Multifuge 3SR, Thermoscientific, Waltham, MA, USA with Sorvall Heraeus 75,006,445 swinging bucket rotor).

The <2 μm fraction was extracted through sedimentation from the purified Na-saturated material in a climate-controlled environment (20°C), following Stokes' law and using the specific density of quartz (2.65 g/cm^3). For optimal saturation of the <2 μm fraction, high purity NaCl salt was introduced to the suspension to attain an overall Na concentration equivalent to 50 times the calculated CEC of the smectite as recommended by Steudel and Emmerich (2013). Reaction time of 24 h was allowed, then the solid part was retrieved by centrifugation. Saturation with NaCl was repeated three times, followed by a thorough washing (via centrifugation) with deionized water. Tthe excess of salt was eliminated through dialysis (6 KDa membranes), continuing until a negative silver nitrate test was achieved in the immersing water.

Henceforth, the notations BSU >2Na and BSU <2Na are used for Na^+-saturated fractions of Secursol UHP, and BC >2Na and BC <2Na for the Na^+-saturated fractions of Calcigel. While the raw (granular)

materials are referred to with their full names.

2. Methods

2.1. X-Ray Diffraction (XRD)

Random powder mounts were prepared from 2 g of material ground in ethanol for 10 min using a McCrone mill. (McCrone, Westmont, IL, USA) and passed through a 20 μm sieve. Textured slides were prepared from the supernatant (collected after 5 min) of 100 mg ground material dispersed in 5 mL deionized water. XRD patterns were recorded by a Bruker D8 Advance A25diffractometer (Bruker AXS GmbH, Karlsruhe, Germany) with a LynxEye XE detector, a variable slit, and Soller slits (primary and secondary) of 2.5°, using CuKα radiation and a sample rotation of 15/min, and a step-size of 0.02° and step-time of 3 s. Oriented slides were analyzed in the air-dried (AD) state (ambient humidity and room temperature), and following equilibration over ethylene glycol (EG) for 24 h at 60 C. Qualitative analysis was performed using the EVA software (Bruker GmbH), and quantitative phase analysis (QPA) performed using Profex 5.2.1 BGMN (Doebelin and Kleeberg, 2015).

The number of layers in stacks (*D*), which corresponds to coherent scattering domain (CSD) in the direction propped by X-ray beam (i.e., c-axis in textured samples), were calculated from the textured EG-saturated XRD patterns for both materials using Sherer equation as detailed in Weidenthaler (2011).

2.2. X-Ray Fluorescence (XRF)

Major elements were determined using an Axios spectrometer (Malvern Panalytical GmbH, Kassel, Germany) equipped with a rhodium X-ray tube at 2.4 kW. Powdered samples were fused with lithium tetraborate (1:14 mixing ratio) and loss on ignition (LOI) was determined separately at 1000°C (2 h).

The reported structural formulas were calculated based on 12 oxygen atoms per formula unit and taking into consideration the measured mean LC according to Köster (1977), and Wolters et al. (2009), using XRF results of the BC <2Na and BSU <2Na samples after removing impurities determined by QPA (Wolters et al., 2009).

2.3. Layer charge (LC)

The mean value and density of the layer charge of the smectite phase in the bentonite was determined according to the alkylammonium method (Lagaly, 1981). Fourteen alkylammonium formate solutions (0.1 M) were prepared according to Lagaly (1994) with alkyl chain lengths ranging from 4 to 18C, except 17. For every chain length solution, two exchange cycles were performed with 100 mg of the raw bentonite in 100 mL formate solution; the samples were left to react at 60°C. After 2–3 d, the solid was separated by centrifugation (10 min, 4500 rpm), washed with ethanol, again dispersed in fresh alkylammonium solution. After saturation, the excess formate was washed with pure ethanol (16×). Finally, 10 wt% of muscovite standard was added and dispersed in 3 mL ethanol. The mixture was pipetted onto a glass slide and dried overnight in a desiccator above P_2O_5 solution before the XRD measurements recorded between 2 and 12° 2θ with a step size of 0.04° 2θ/8 s.

2.4. Cation Exchange Capacity (CEC) and Exchangeable Cations (EC)

CEC was determined following the *Cu*-triethylenetetramine (Cu-trien) method (Meier and Kahr, 1999). 50–60 mg of sample were dispersed in 5 mL Cu-trien solution (0.01 M) and 10 mL deionized water, shaken for 3 h before centrifuging at 4500 rpm for 10 min. Absorbance maxima of the supernatant at 580 nm were measured using a UV–Vis spectrophotometer (Genesys 10 UV, Thermo Electron Corporation, Waltham, MA, USA). Exchangeable cations (Na^+, K^+, Ca^{2+}, Mg^{2+}) were measured in 5 mL of the supernatant, diluted to 9.75 mL with deionized and acidified by adding 0.25mL of 1 M HNO_3, using inductively coupled plasma-optical emission spectroscopy (ICP-OES, Optima 8300 DV, Perkin Elmer Inc., Waltham, MA, USA).

2.5. Electrical conductivity and soluble salts

2 g of the raw bentonite were dispersed in 40 mL of deionized water, swirled for 24 h, then centrifuged for 10 min at 4500 rpm. Conductivity and temperature were measured concurrently in the supernatant with a WTW LF 318 (Xylem Analytics Germany Sales GmbH and Co. KG, Weilheim in Oberbayern, Germany). Conductivity, χ, was converted to conductivity at 25°C ($\chi_{25°c}$) according to $\chi_{25°c} = \frac{\chi}{1+\alpha(T-25)}$, where α is the temperature coefficient of water at ~0.021 and T is the temperature in °C. Soluble anions concentrations (Cl^-, NO_3^-, and SO_4^{2-}) were measured from filtered supernatant (45 μm syringe filter) using A Dionex Aquion (Thermo Fisher scientific GmbH, Karlsruhe, Germany), equipped with IonPac™ AG23 RFIC™ and AS23 RFIC™ guard and analytical columns and a Dionex AERS 500 Carbonate 4 mm suppressor using a sodium carbonate/bicarbonate (4.5/0.8 mM) solution as the eluent and a Dionex AS-DV Autosampler. Soluble cations concentrations were measured using ICP-OES under the same conditions described in the CEC section.

2.6. N_2, water vapor, and polar liquid adsorption

N_2 adsorption isotherms were recorded at 77 K using Quantachrome autosorb-1 analyzer. Before measurements, samples were outgassed at 150°C for 24 h. Specific surface area (a_s (N_2)) was calculated according to the BET method (Brunauer et al., 1938) in the adsorption range of 0.04–0.2 p/p_0.

Water adsorption isotherms were recorded using Quantachrome Hydrosorb 1000 device. 60–100 mg of sample were outgassed at 105°C and adsorption / desorption isotherms were recorded at 20°C between a relative humidity of 2.5 % and 95 % with total of 44 points.

Adsorption of the polar molecule ethylene glycol monoethyl ether (EGME) was determined according to Carter et al. (1965) and Cerato and Lutenegger (2002). 1 g of ground raw bentonite dried at 120°C for 48 h, homogenized with 3 mL EGME by swirling, subjected to a vacuum of 635 mmHg (0.085 MPa) and weighted to mass equilibrium (<0.001 g). Comparison of the adsorbed mass of EGME with the initial mass allows for determination of the total specific surface area (a_s (EGME)) including interlayer and external surface, assuming that 0.000286 g are required to form a monomolecular layer of adsorbed EGME on an area of 1 m^2.

2.7. Simultaneous thermal Analysis (STA)

STA was performed using a Netzsch STA 449C Jupiter (Netzsch Holding, Selb, Germany) equipped with a thermogravimetric/differential scanning calorimetry (TG/DSC) sample holder and a 403C Aëolos quadrupole mass spectrometer (Netzsch Holding, Selb, Germany) to detect m/z = 18, 44, and 64 (H_2O, CO_2 and SO_2 respectively). Before measurements, the samples were stored at 20°C in a desiccator for a week at 54 % relative humidity (*r.h.*), using saturated Mg $(NO_3)_2$ solution (Winston and Bates, 1960)0.100 mg of sample were heated from 35 to 1100°C at a rate of 10 K/min with N_2 as the protective gas (20 cm^3/min) and synthetic air (SA) as purge gas (50 cm^3/min). Pt80Rh20 crucibles with punctured lids, and an empty crucible with lid used as the reference. Dry weight of sample following dehydration was used to normalize the remainder of the TG curve. The dehydroxylation of *cis*-vacant (*cv*) dioctahedral smectites occurs between 650 and 700°C, while for *trans*-vacant (*tv*) dioctahedral smectite, it occurs between 500 and 550°C (Tsipursky and Drits, 1984; Drits et al., 1995; Drits and Zviagina, 2009). Therefore, the ratio of *tv:cv* octahedral sheets of the smectite phase was estimated from the area ratio of the fitted dehydroxylation peaks in mass spectrometer (MS) curve of evolved water (m/z = 18)

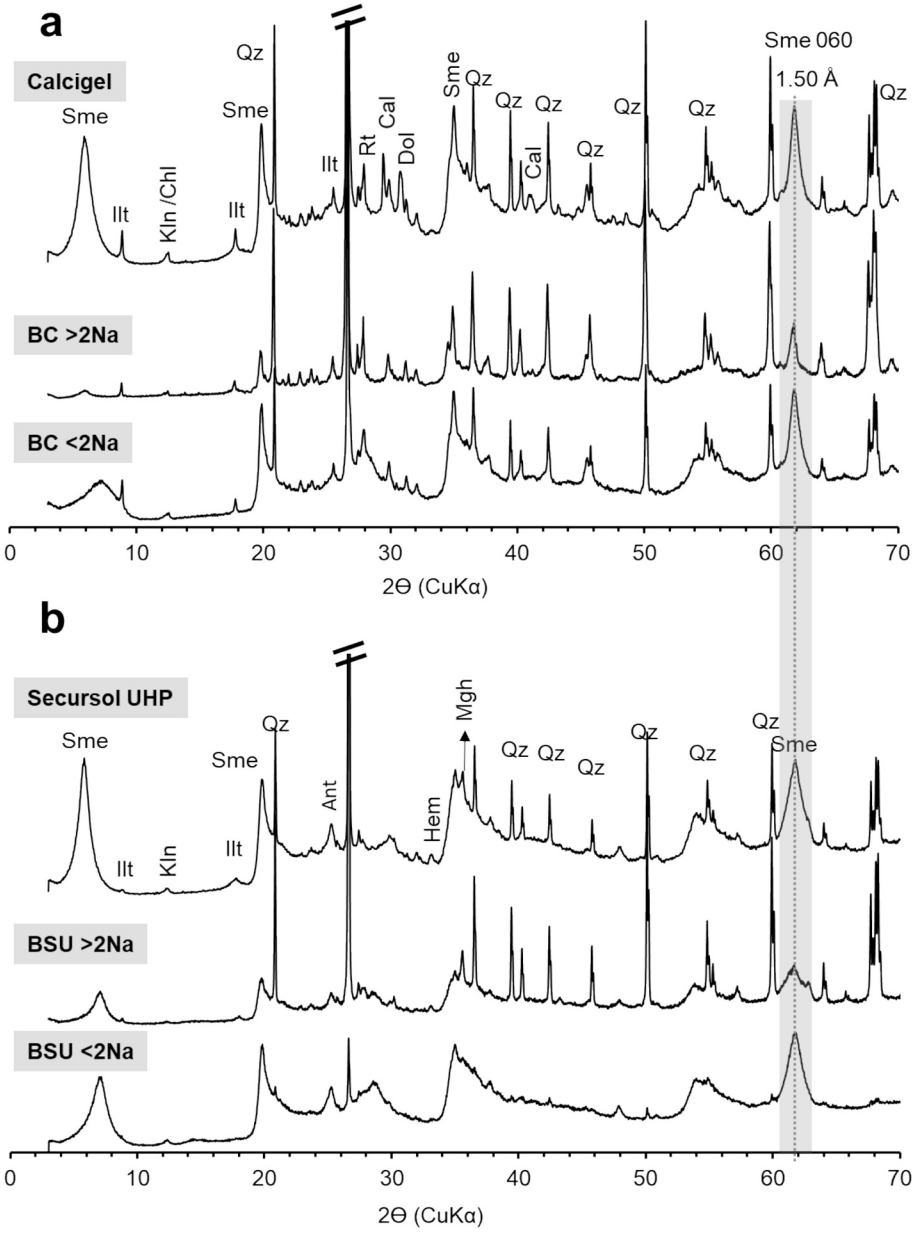

Fig. 1. XRD from randomly oriented powders of Calcigel (BC) and Secursol UHP (BSU) and their size fractions. Sme = smectite (di), Ilt = illite/mica (di), Chl = Chlorite, Kln = Kaolinite, Qz = Quartz, Rt = Rutile, Cal: Calcite, Dol: Dolomite, Ant = Anatase, Hem: Hematite.

between 400 and 800°C (Fig. S2, supplementary data). The boundary between *cv* and *tv* dehydroxylation was set at 600°C, following the methodology of Wolters and Emmerich (2007).

2.8. Atomic Force Microscopy (AFM)

AFM studies were performed using Cypher S device (Asylum Research, Oxford instruments, USA) equipped with AC106TSA Cantilever. 50 mg/L dispersions of the Na-saturated <2 μm samples were prepared through 15 min of ultra-sonication (37 kHz). 40 μL of dispersion was placed over freshly cleaved muscovite surface, the excess of solution was removed, and 0.1 M NaCl solution was added immediately before starting the measurements. Recording was in none-contact AC mode. AFM images were processed using Gwyddion modular free software (http://gwyddion.net/). The following parameters were directly extracted for each particle; thickness (h), equivalent disc diameter (d_d), minimum and maximum Martin diameter (i.e., minimum and maximum length of the area bisector of the particle) from which the average value (d_m) and ratio minimum to maximum (R_m) were calculated, equivalent square side (S_d), the basal area (A), and the perimeter (P). Assuming that particles (single 2:1 layer of smectite) are 1 nm thick and disclike shaped with 100 to 200 nm diameter, the uncertainties of particle height caused by lateral AFM tip artifact was estimated at 3–5 % for 1–2 nm particle height according to Plaschke et al. (2001) and using tip radius of curvature (R_t) of 7 nm according to the manufacturer's specification. Measured particle perimeter and basal area uncertainties were estimated to 4–5 % and 7–10 %, respectively, based on diameter uncertainty.

The weighted main value of each parameter was calculated to account for particle size distribution influence, as detailed in Delavernhe et al. (2015) following the work of Plaschke et al. (2001), and Tournassat et al. (2003). For the weighted main values, the specific density (ρ_s) of smectite in Calcigel and Secursol UHP was calculated as 2.75 and 2.79 g/cm^3, respectively, based on phase content and crystal structure from XRD. The specific surface area was calculated using either the average weighted disk or the square side values and the number of layer

Table 2
CEC, exchangeable cations (EC), electrical conductivity of the suspension, and soluble ions of Securosol UHP (BSU) and Calcigel (BC) bentonites.

	CEC													
	[cmol(+)/kg] ± 1	w_{min}	Exchangeable cations											
		200°C, 24 h	Mg^{2+}	Ca^{2+}	Na^{+}	K^{+}	Fe^{3+}	Mg^{2+}	Ca^{2+}	Na^{+}	K^{+}	Fe^{3+}	Sum	% CEC
		[%] ± 1	[mg / g] ± 1					[cmol (+) kg-1] ± 1						
Secursol UHP	88.0	15.1	2.6	13.4	0.5	0.3	0.0	21.2	66.8	2.3	0.8	0.0	91.1	103.6
BSU >2Na [a]	55.0	2.3	0.1	0.8	12.3	0.1	0.0	0.7	4.0	53.6	0.2	0.0	58.5	106.4
BSU <2Na [a]	93.0	12.6	0.2	0.7	22.2	0.2	0.0	1.4	3.6	96.7	0.5	0.0	102.2	109.9
Calcigel	60.0	10.5	2.2	8.3	0.7	0.4	0.0	18.5	41.5	2.9	1.0	0.1	63.9	106.4
BC >2Na [a]	20.0	2.3	0.0	26.2	0.9	0.1	0.0	0.3	130.6	4.0	0.2	0.0	135.1	675.5
BC <2Na [a]	63.0	5.6	0.3	0.3	14.3	0.4	0.0	2.1	1.4	62.1	1.1	0.0	66.6	105.6
	Electrical Conductivity													
	[µS/cm] ± 2		Soluble ions											
Secursol UHP	75.0		0.1	0.2	0.2	0.0	0.1	0.6	1.1	1.0	0.1	0.4	3.1	3.5
Calcigel	119.0		0.1	0.2	0.4	0.1	0.0	0.5	0.8	1.6	0.1	0.1	3.1	5.2
			Cl^{-}	SO_4^{-2}	NO_3^{-}			Cl^{-}	SO_4^{-2}	NO_3^{-}				
Secursol UHP			0.1	0.4	0.0			0.2	0.8	0.04				
Calcigel			0.1	0.1	0.0			0.2	0.2	0.05				

[a] < or > 2Na refer to the less or more than 2 µm Na-saturated size fraction.

stacks (*D*) from XRD.

2.9. Methods for geotechnical classification tests

The geotechnical classification was carried out on the granular material (i.e., as received) according to DIN EN ISO standards (Deutsche Institut für Normung e.V.), which represent the European and international harmonized standards. The grain density (ρ_s) was measured by capillary pycnometer method (DIN EN ISO 17892-3, 2016), as an average of five measurements and drying at 105°C. The water and moisture content, referring the mass of water to oven dried and wet bentonite mass, respectively, were determined by oven drying at 105°C (DIN EN ISO 17892-1, 2015) and 200°C. The particle size distribution was determined by (*i*) a combined sieve and sedimentation analysis on the entire fraction, (*ii*) a sedimentation analysis on the entire fraction of the granular material and (*iii*) a sedimentation analysis on the fines fraction <0.063 mm of the granular material (DIN EN ISO 17892-4, 2017). For sedimentation, the material was dispersed in 0.045 M tetrasodium pyrophosphate decahydrate ($Na_4P_2O_2$*$10H_2O$) and stirred prior to the sedimentation analysis to ensure dispersion. The geotechnical classification was carried out according to DIN EN ISO 14688-2, 2020based on the Atterberg limits determined according to DIN EN ISO 17892-12, 2020and DIN 18122-2:2020-11, 2020. The liquid limit (w_L) was determined with the Casagrande and the fall cone methods. For both methods, granular material with different water contents in the range of w = 85 to 100 % for Secursol UHP and w = 110 to 135 % for Calcigel were manually mixed and left to homogenize in closed containers for several days before testing. From the measured Atterberg limits, the plasticity index, I_P and the consistency index, I_C were calculated. The water uptake of the materials was tested on manually milled material, gently dried to 60°C, according to (DIN 18132) in an Enslin-Neff device considering the evaporation correction of Kugler et al. (2002) and Kaufhold and Dohrmann (2008). Finally, the swell index was determined according to ASTM D5890 on manually milled material, oven dried at 105°C.

3. Results and discussion

3.1. Calcigel and Secursol UHP mineralogy and intrinsic properties

Calcigel and Secursol UHP exhibit similar major mineralogical phases but in different proportions (Table 1); Secursol UHP has 20 % higher smectite content and considerably less quartz and dioctahedral mica/illite. Calcigel exhibit 4.4 wt% calcite and dolomite, while carbonates were not detected by XRD in Secursol UHP (Fig. 1). The 060 reflection of smectite at 1.50 Å (Fig. 1) suggests the dioctahedral structure of the smectite in both bentonites (Brindley and Brown, 1982). This mineralogical composition is consistent with what is reported in the literature for both bentonites (summarized in Table 1). In addition, QPA results (Table 1) show that the homoionic <2 µm fractions are carbonate free and the smectite content increases by 12–16 wt%. The minor mineralogical phases, however, differ. For instance, Secursol UHP contains 2–3 wt% of anatase, a low-temperature polymorph of TiO_2 (Deer et al., 2013), with traces of rutile, the high-temperature polymorph, likely of detrital origin. On the other hand, Calcigel contains only small quantity of the high-temperature polymorph rutile. This could be an indication that Secursol UHP underwent lower alteration temperatures compared to Calcigel. Moreover, Secursol UHP contains iron oxides, unlike Calcigel, suggesting more basic basaltic source-rocks, this observation is also validated by the similar trace elements content of Westerwald bentonite and the overlying basalt as reported in Fontaine et al. (2020). Furthermore, these authors argued that the absence of vertical mineralogical or geochemical variation in the Westerwald bentonite indicates that surficial weathering was fundamentally not involved in its formation, and that the overlying basalt likely helped it to preserve the fabric of its precursor. Evidence of this 'inherited fabric' in Secursol UHP can also be seen in a report on Westerwald bentonite by the German Federal Institute for Geosciences and Natural Resources (BGR) (Dohrmann, 2012). Indeed, SEM investigation on unprocessed material shows how smectite particles are densely enclosed inside a shell of the remaining structure of their precursor mineral (image is provided in supplementary data). On the contrary, Calcigel, most probably has been formed through alteration of acid vitreous tuff which was transported from farther locations (Grim and Güven, 1978; Weinig, 1987; Unger et al., 1990; Ulbig, 1994, 1999; Aziz et al., 2010, with more details in the supplementary data). Such formation conditions significantly deteriorate the texture of the precursor minerals.

CEC values (Table 2) for Calcigel and Secursol UHP fall within the range reported in the literature (Table 1). For both bentonites and their size fractions, the CEC correlates with the smectite content, confirming that it is practically the only phase responsible for the CEC. The smectite phase in both bentonites is Ca/Mg-saturated with minor amounts of sodium and potassium, as confirmed by EC results (Table 2). The Ca:Mg ratio is higher in Secursol UHP at 3.2:1 compared to Calcigel at 2.2:1, aligning with the findings of Bohác et al. (2019) and Emmerich et al. (2021). Additionally, EC results from the size fractions of both bentonites confirm the successful homoionic exchange process, with Na^{+} concentration comprising about 95 % of the measured EC.

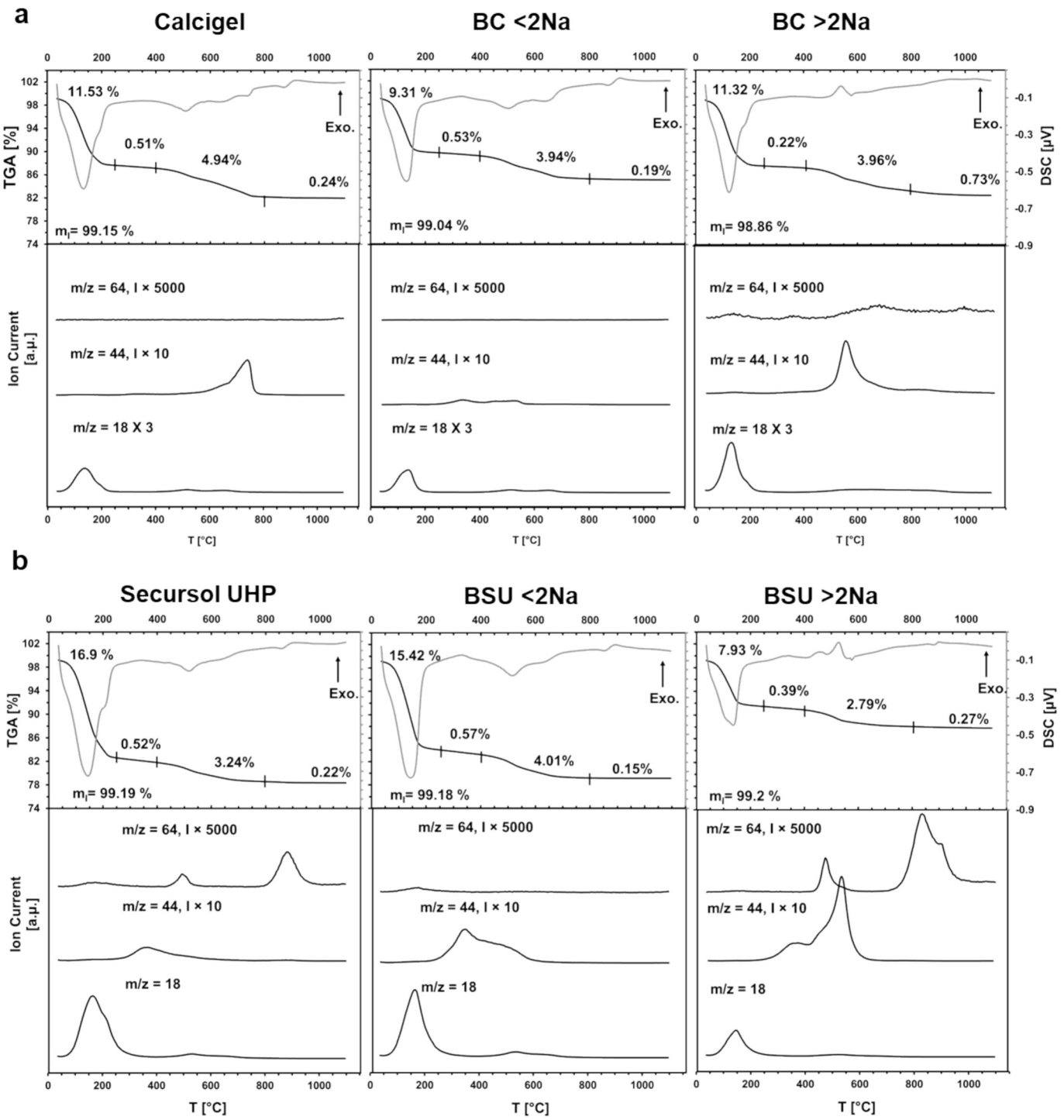

Fig. 2. TGA, DSC, and mass spectrometry results for (a) Calcigel (BC), and (b) Secursol UHP (BSU), and their size fractions.

Electrical conductivity for Secursol UHP in suspension (Table 2) is two times higher than reported in Emmerich et al. (2021), and slightly lower than what is reported for Calcigel in Emmerich et al. (2019) (150 µS/cm). Soluble Ca and Mg are lower compared to EC as Cu-trien during CEC measurement increases solubility of carbonates compared to deionized water (Bohác et al., 2019).

STA results are shown in Fig. 2 for both raw bentonites and their subfractions. The mass loss in the TG curve, between 35 and 250°C correlates with evolved water ($m/z = 18$) due to the evaporation of adsorbed water and dehydration of exchangeable cations in the smectite interlayer. In this range, the double endothermic reaction suggests that the raw materials are in 2 W state, consistent with the presence of divalent cations (Greene-Kelly, 1957; Smykatz-Kloss, 1974). The Na-saturated sub-fractions for both bentonites show a single endothermic reaction, indicating a 1 W state and monovalent interlayer cations. The mass loss is greater for Secursol UHP than Calcigel, reflecting its higher smectite and moisture / water content. Both bentonites and their sub-fractions show a second mass loss due to an exothermic reaction around 350°C, associated with CO_2 release from organic matter oxidation. This CO_2 peak may originate from the raw material, seen in raw Secursol UHP, or be inherited from volatile chemicals of plastic equipment used during treatment, as in BC <2Na. Additionally, in CG >2Na and BSU

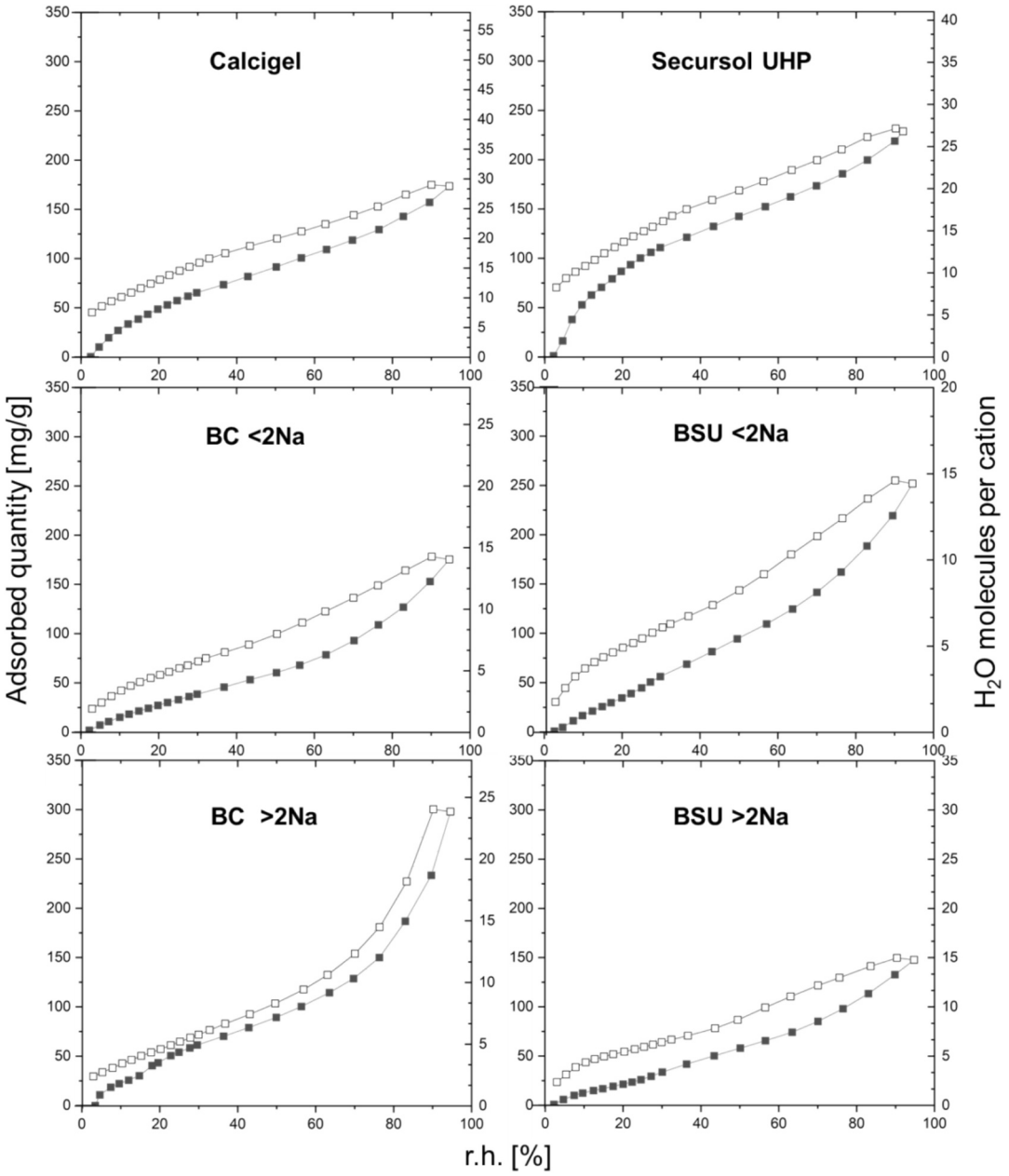

Fig. 3. Water adsorption isotherms results for Calcigel (BC) and Securesol UHP (BSU) and their size fractions.

>2Na, a CO_2 peak observed at 530–550°C is accompanied by both exothermic and endothermic signals on the DSC curve. While this pattern resembles the decomposition of siderite (Emmerich and Smykatz-Kloss, 2002), siderite was not detected by XRD. Even if present in trace amounts, it is unlikely to withstand the pre-treatment applied to these fractions. Therefore, to avoid speculation, further investigation is needed. The mass loss associated with carbonate decomposition in Calcigel (Fig. 3a) occurs as an endothermic reaction around 750°C and is accompanied by two overlapping CO_2 peaks ($m/z = 44$) at the same temperature. The first, broader peak corresponds to the decomposition of $MgCO_3$ from dolomite, while the second, at a slightly higher temperature, reflects the decomposition of $CaCO_3$ from both calcite and dolomite (Emmerich, 2010). No similar reaction can be observed for Securesol UHP. Additionally, In the MS curve of m/z = 64 of Securesol UHP and BSU >2Na, two SO_2 releases can be detected, first one at 475–490°C which can be assigned to pyrite oxidation, and another release at 850–900°C which can be tentatively assigned to reaction of evolved SO_2 with the Ca in the remaining solid samples, mimicking sulfate that was not in the raw material (Emmerich, 2010).

Water adsorption and desorption isotherms are shown in Fig. 3. The number of water molecules per exchangeable cation (right vertical axis), were obtained by recalculating the adsorbed water (mg/g) to number of H_2O molecules/g and divide it by the number of released cations per g of material calculated from EC results (Table 2). All isotherms exhibit a hysteresis loop with nearly parallel adsorption and desorption branches. The largest loop and fewer parallel branches are seen in material saturated with monovalent cations (e.g., Na), while material with divalent cations (e.g., raw bentonites) shows a narrower loop with more parallel branches. All samples retain some water at the end of the desorption branch at the lowest *r.h.* values (2–2.5 %), with more significant retention in materials containing divalent interlayer cations. This observation can be attributed to the higher hydration energy of divalent cations compared to monovalent ones. In addition, the retained water may require *r.h.* values between 0.5 and 0.9 % to completely remove

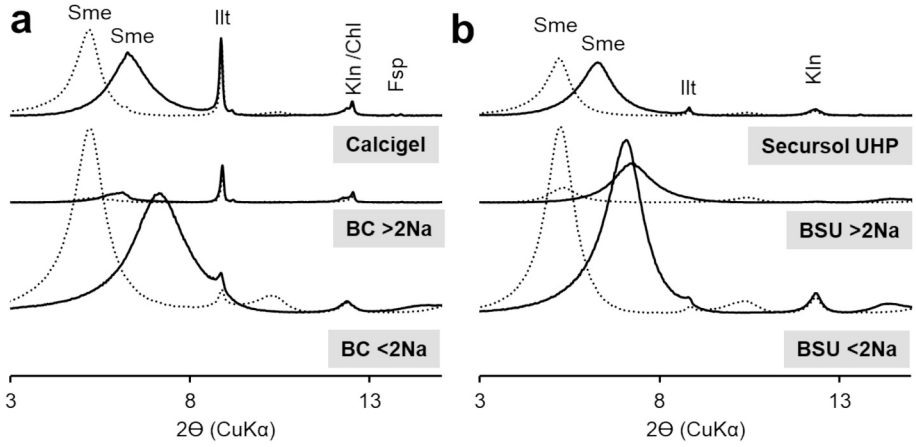

Fig. 4. XRD from textured preparations. Air dry (AD, solid lines), and after ethylene glycol saturation (EG, doted lines). (a) Calcigel (BC), (b) Secursol UHP (BSU). Sme = smectite (di), Ilt = illite/mica (di), Chl = Chlorite, Kln = Kaolinite, and Fsp = Feldspar.

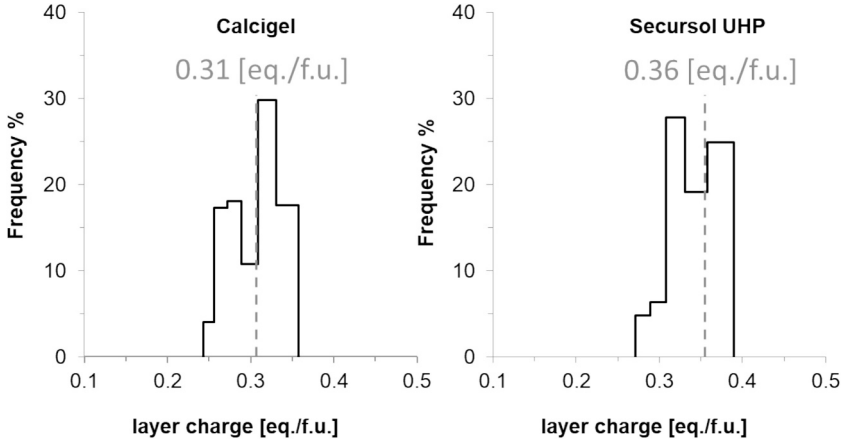

Fig. 5. Layer charge density distribution and average values for the smectite phase in Calcigel and Secursol UHP.

water from Na-montmorillonite with similar layer charge to the material in this study as indicated by Density Functional Theory (DFT) calculations in Emmerich et al. (2018). At *r.h.* = 56 %, approximately the ambient humidity during measurements and storage conditions, the Na-saturated sub-fractions of both bentonites have 5–6 water molecules per interlayer cation, corresponding to the formation of one layer of water molecules in the interlayer of smectite, confirmed by the d_{001} of 12.5 Å in the XRD data (Fig. 2). This value is consistent with what is published in the literature on water organization in the interlayer of smectite, as seen in the work of Bradley et al. (1937), Ferrage (2005), Ferrage et al. (2010), and Emmerich et al. (2018). On the other hand, both raw bentonites have 17–18 water molecules per interlayer cation, which is higher than the 11–12 water molecules per cation normally reported in the literature. This discrepancy could be due to the contribution of other phases in the raw material or the presence of water in the porosity.

3.2. Calcigel and Secursol UHP smectite phase properties

Under AD conditions in XRD textured preparation (Fig. 4; solid lines), the position of the 001 basal reflections of smectite in both bentonites is around 15 Å, in agreement with two water layers (2 W) hydration state, at ambient conditions, and the presence of the divalent, Ca^{2+} and Mg^{2+}, interlayer cations (Ferrage, 2005). In the Na-saturated fractions, the 001 reflection of smectite is between 12.3 and 12.5 Å, reflecting the presence of monovalent (Na^{+}) interlayer cation in (1 W) hydration state at ambient conditions (Ferrage, 2005; Ferrage et al., 2010; Emmerich et al., 2018). For both bentonites, the 001 of smectite shift to 16.9–17.1 Å after EG saturation (Fig. 4; dashed lines) indicating that the smectite is a pure phase without interstratification with other layer types.

Smectite layer charge density (Fig. 5) ranges from 0.24 to 0.36 for Calcigel, and 0.27 to 0.39 eq/f.u. for Secursol UHP. The average values (Table 1) indicate low layer charge smectite in both bentonites (Emmerich et al., 2009b). The average layer charge value for Calcigel is in agreement with 0.30 eq/f.u. reported in Delavernhe et al. (2015). To the extent of our knowledge, no similar data were reported for Secursol UHP.

The structural formula of the smectite phase in each bentonite are reported in Table 3. They are in agreement with ones reported in Delavernhe et al. (2015) for Calcigel, and Fontaine et al. (2020) for bentonite from Westerwald similar to Secursol UHP. They show that both smectites are mainly dioctahedral with substantial tetrahedral charge (i.e., 57 and 76 % for smectite of Calcigel and Secursol UHP, respectively; Table 3). Hence, both can be classified as montmorillonitic beidellite (Emmerich et al., 2009b). The ratio of octahedral to tetrahedral charge in smectite of Calcigel is close to 50:50, therefore other batches with slightly lower tetrahedral charge were classified as beidellitic montmorillonite as in Wolters et al. (2009) and Delavernhe et al. (2015). Both smectites contains iron with noticeably higher content in Secursol UHP leading to slightly higher molar mass and specific density per f.u (Table 3). In addition, the proportion of *trans*- to *cis*-vacancies in the octahedral sheets of dioctahedral smectites (Table 3) show that

Table 3
Chemical composition of the major elements [wt%] (normalized to 100 %), structural formulae of smectites after impurities correction based on $O_{10}(OH)_2$.

Oxide [Wt%]		Securosol UHP			Calcigel		
		Raw	<2Na[a]	>2Na[a]	Raw	<2Na[a]	>2Na[a]
SiO_2		61.85	58.53	69.26	63.06	64.12	70.32
TiO_2		2.71	2.56	3.04	0.72	0.73	1.12
Al_2O_3		16.90	19.68	10.80	20.30	20.99	15.33
Fe_2O_3		11.45	11.32	11.50	6.72	6.95	4.57
CaO		2.51	0.26	0.41	3.20	0.23	3.31
MgO		3.43	3.33	2.09	3.54	2.66	1.60
K_2O		0.97	0.93	0.90	2.05	1.94	2.89
Na_2O		0.18	3.39	2.00	0.41	2.38	0.86
Tetrahedral sites							
Si	[mol/f.u.]		3.72			3.83	
Al^{IV}			0.28			0.17	
ξ	[eq./f.u.]		0.28			0.17	
Octahedral sites							
Al^{VI}	[mol/f.u.]		1.18			1.34	
Fe^{3+}			0.57			0.41	
Mg			0.33			0.31	
∑ Oct.			2.08			2.06	
ξ	[eq./f.u.]		0.09			0.13	
Exchangeable sites							
Ca^{2+}	[mol/f.u.]		0.02			0.01	
Na^+			0.30			0.23	
K^+			0.05			0.06	
ξ	[eq./f.u.]		0.37			0.30	
Classification							
Tetrahedral charge of total charge		76.00 %			57.00 %		
Mineral name		Montmorillonitic Beidellite			Montmorillonitic Beidellite		
Octahedral distribution							
$W_{tv/cv}$	*tv/cv* [%]	63–65.00 / 35–37.00			53–57.00 / 43–47.00		
Fe of octahedral cations		38.00 % (Ferric)			25.00 % (Ferric)		
Molar mass	[g/mol]	386.00			381.00		
ρ_s	[g/cm^3]	2.792			2.754		

[a] < or > 2Na refer to the less or more than 2 μm Na-saturated size fraction.

octahedral sheets in smectite from Calcigel are *tv / cv* = 53–57 / 43–47 in agreement with results reported in Delavernhe et al. (2015) (*tv / cv* = 56/44). While for the smectite in Securosol UHP the ratio is *tv / cv* = 63–65 / 35–37. Hence, Securosol UHP exhibits approximately 10 % higher trans-vacant occupancies in the octahedral sheet compared to Calcigel. In line with the observation in the previous section, this could also indicate that Securosol UHP formed under more stable physico-chemical conditions (Drits and Zviagina, 2009). Moreover, the high tetrahedral substitutions and Fe-rich octahedral sheets in the smectite in Securosol UHP (Table 3) reflects its basaltic precursor (Fontaine et al., 2020), which is also relatively low in Si and Al. Conversely, smectite in Calcigel exhibits significant tetrahedral substitutions and an Fe-rich octahedral sheet, which does not necessarily reflect the composition of rhyolitic tuff precursor rich in Si and Al. It is also Ca/Mg-saturated, despite rhyolitic tuff being known for its low Ca and Mg content. While this has been attributed to the circulation of Ca-Mg-rich meteoric waters during bentonitization (Gilg and Ulbig, 2017; Köster et al., 2017), this explanation does not account for the relatively high Fe content.

Smectite morphological properties from AFM are shown in Fig. 6. Single smectite layers were identified based on their height by coupling height and amplitude images Fig. 6a & b. The morphology of individual layers ranges from irregular, angular shapes to more elongated, rectangular forms, particularly evident in Calcigel. Smaller layers frequently exhibit rounded shapes, which are more commonly observed in Secursol UHP (Fig. 6b). Given that the thickness of an individual smectite layer with charge balancing cations (i.e., Na) is about 0.96 nm, and the average height of analyzed individual layers ranged from 1.1 to 1.3 nm, this suggests a formation of an average of one water layer between the particle and the muscovite substrate (Tournassat et al., 2003; Cadene et al., 2005). The size distribution of individual smectite layers (Fig. 6c) was calculated based on three possible particles shapes deduced from the measured basal area of the particle (Table 4): $\overline{d_d}$, $\overline{d_m}$, and $\overline{S_d}$ (definitions are in section 2.8). Although there is a good agreement between $\overline{d_d}$ and $\overline{d_m}$ for the same material suggesting that particles have rounded basal surfaces. However, the ratio $\overline{R_m}$ in Calcigel and Secursol UHP is 0.47 and 0.54, respectively (Table 4), Indicating that the smectite particles likely have elliptical/rectangular shapes. Therefore, the Martin diameter with the R_m ratio is more representative of the actual basal morphology of the particles than the average disc diameter commonly used in literature. On the other hand, $\overline{S_d}$ values tend to yield slightly higher values than $\overline{d_d}$ and $\overline{d_m}$ in the low range, and lower values in the high range. Nevertheless, the distribution ranges between 25and 150 nm for smectite of Secursol UHP with a mean average weighted disc diameter of 95 nm ($\overline{d_d}$; Table 4). A relatively larger distribution is observed for smectite of Calcigel between 1 and 225 nm and $\overline{d_d}$ = 126 nm. The mean weighted perimeter/basal area ratio $\overline{R_{P/A}}$ is similar for smectites of both bentonites at 0.05 and 0.06 nm^{-1} for Calcigel and Secursol UHP, respectively. For the smectite in Calcigel, the distribution, ratio $R_{P/A}$, and average diameter are in good agreement with what is reported in Delavernhe et al. (2015) ($\overline{d_d}$ =118 nm, $\overline{R_{P/A}}$ = 0.054 nm^{-1}). The total specific surface area of single layer (a_s (0.96 nm)) was calculated to be 758 and 747 m^2/g for smectite of Calcigel and Secursol UHP, respectively. The edge surface area ($a_{s,\ edge}$, Table 4) is rather low, at less than 4 % for both smectites. For comparison purpose, a_s (N_2) for the <2 μm fractions of both bentonites (Table 1) can be scaled to 100 % smectite content, considering that this average value is mainly derived from smectite particles in the bentonite. By doing so, the a_s (N_2) can be estimated at 102 and 112 m^2/g for Calcigel and Secursol UHP, respectively (Table 4). Using the calculated average weighted diameter values ($\overline{d_d}$ and $\overline{d_m}$) and a_s (N_2), the layer stacking of dried Na-saturated powder can be estimated at 8 and 9 layers for smectite in Calcigel and Secursol UHP, respectively as shown in Fig. 6d. Interestingly, these values are similar to number of layers in stack (*D*) reported in Table 1 for the same samples (<2 Na). Similar to a_s (N_2), a_s (EGME) was scaled to 100 % smectite content Table 4, from a_s (EGME) corresponding to the bulk material (Table 4). From the good agreement between a_s (0.96 nm) and a_s (EGME) It can be concluded that EGME is fully absorbed both in the interlayer and on the outer surfaces. Nevertheless, sorption of polar EGME like water strongly depends on the type of the exchangeable cation resulting in different cross-sectional areas (Kellomäki et al., 1987; Chiou and Rutherford, 1997), and thus, it measures only an apparent specific surface area.

Finally, it should be noted that the sample BC >2Na represents a unique case in this study. It exhibits low smectite content (27 %) evident in its low cation exchange capacity (CEC) at 20 cmol(+)/kg, yet it releases a high amount of Ca^{2+} in the CEC solution (Table 2) at twice the amount found in the raw material. Additionally, it demonstrates a relatively high-water adsorption capability (Fig. 4). The smectite phase in this size fraction appears to remain Ca-saturated, as evidenced by the weak 001 reflection of smectite at 14.8 Å (AD) and the double endothermic dehydration reaction observed in its thermogravimetric (TG) curves below 250°C.

3.3. Physico-chemical properties and geotechnical characteristics

The grain density obtained from capillary pycnometer (Table 5) is similar for both bentonites, and in very good agreement with the ones calculated from structural formula of smectite (Table 3). For Calcigel, the geotechnical properties are consistent with ones reported in the

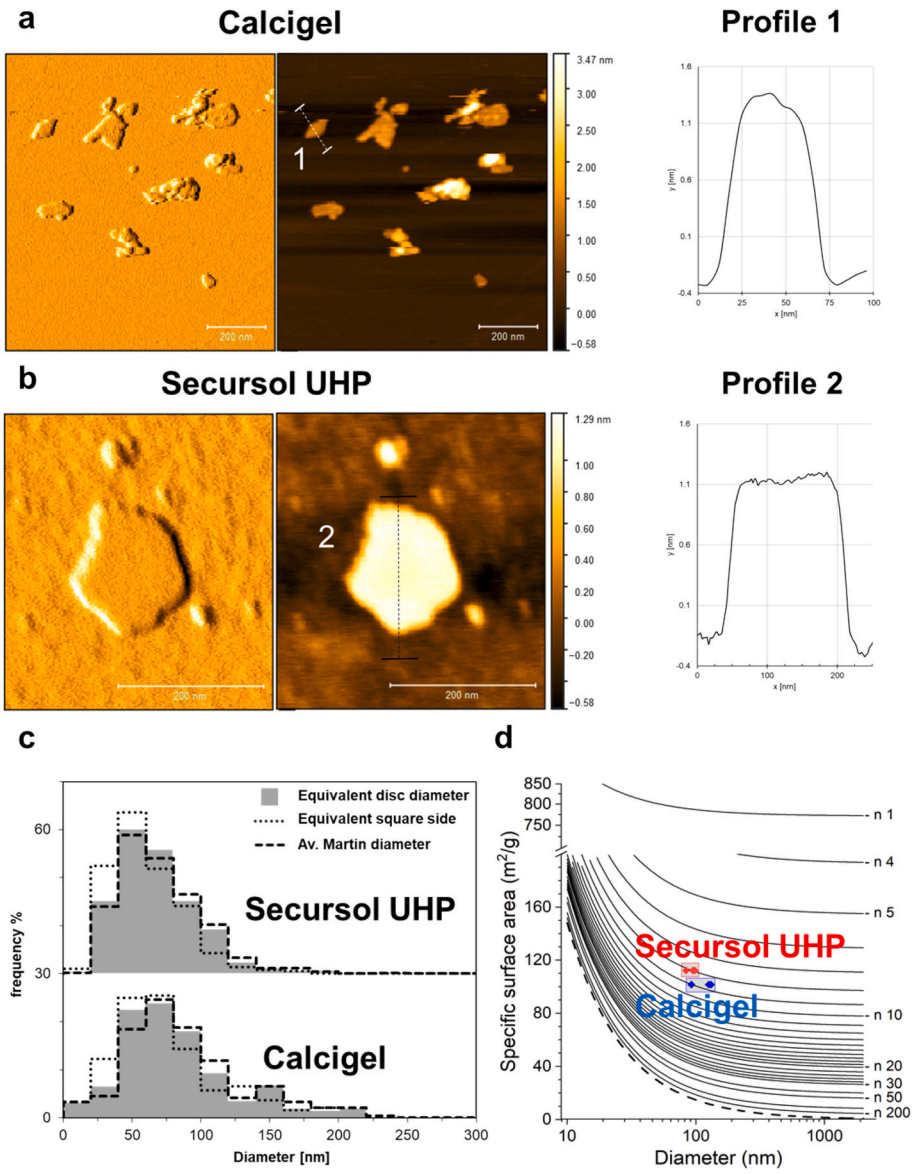

Fig. 6. (a &b) AFM images (Amplitude left, height right) and smectite's particle profile from Calcigel and Securesol UHP <2 μm Na-saturated size fractions. (c) Smectite's particle diameter distribution. (d) Number of layers per stack as function of specific surface area and equivalent disc diameter.

literature (Table 5). Equilibrium water content at ambient conditions in this work is slightly higher (11.9 in comparison to 9–9.5 %). However, Securesol UHP exhibits a higher water content (w) and moisture (w_M) than Calcigel corresponding to its higher smectite content. Water content increases by 4.2 % and 2.7 % for Securesol UHP and Calcigel, respectively when drying temperature is increased from 105 to 200°C (absolute values). Based on exchangeable cation results (Table 2), this difference can be estimated to be approximately 5.5 and 4.6 of remaining water molecules per cation for Securesol UHP and Calcigel, respectively. These values suggest that the material is still in 1 W hydration state after drying at 105°C (Ferrage et al., 2010; Emmerich et al., 2018).

The Atterberg plastic limits of Calcigel are in good conformity with Brenner (1988), Agus and Schanz (2008) and Rawat et al. (2020). In addition, the plasticity index in this study is close to the lower end of the reported range. Nevertheless, it should be noted that granular material was used in this work, whereas the values given in the literature mostly refer to the commercially available powder of Calcigel. Although, it is theorized, that the Atterberg limits are not influenced by the initial state of the material, since it is remolded and homogenized before testing. For Securesol UHP, no literature data exists for comparison. Overall, Casagrande and fall cone method returned similar w_L values for both bentonites.

Although the plastic limit (w_P) is approximately identical for both bentonites, the liquid limit (w_L) for Calcigel is 13–20 % higher than that of Securesol UHP, and thus, the plasticity index ($I_P = w_L - w_p$) is also higher. Both bentonites are classified as highly plastic clays (TA) that exhibit almost identical consistency in their as-received state (similar consistency index $I_C = (w_L - w) / I_p$). The shrinkage limit (w_s) was found to be higher for Securesol UHP compared to Calcigel, though relative to their ambient water contents they are very comparable.

The water uptake according to Enslin-Neff are presented in Fig. 7. The average water uptake of Calcigel is 157 %, considerably higher than that of Securesol UHP (112 %), in line with the higher liquid limit of Calcigel. The swell index of both bentonites is very similar, but contrary to the liquid limit and water uptake it is slightly higher for Securesol UHP (8 mL/2 g) than for Calcigel (7 mL/2 g).

The grain size distribution is displayed in Fig. 8. The results from the combined sieve and sedimentation analysis of the granules (dashed lines) show that Securesol UHP has a slightly finer apparent (or

Table 4
Morphologic parameters from AFM images of smectite's single layer and edge surface area estimation. Calcigel (BC), Secursol UHP (BSU).

Material		BSU <2 Na [a]	BC <2 Na [a]
Particle thickness (h)	[nm]	1.13 ± 0.22	1.32 ± 0.37
Particle count		509.00	244.00
Perimeter ($\overline{P}$)	[nm]	381.00	553.00
E. disc diameter ($\overline{d_d}$)	[nm]	95.00	126.00
Av. Martin diameter ($\overline{d_m}$)	[nm]	98.00	131.00
Min/max Martin diameter ($\overline{R_m}$)	[nm]	0.54	0.47
E. square side ($\overline{S_d}$)	[nm]	84.00	92.00
$\overline{R_{P/A}}$	[nm^{-1}]	0.06	0.05
a_s (0.96 nm)	[m^2/g]	747.00	758.00
$a_{s\ edge}$	[m^2/g]	22.30 ± 4	18.10 ± 3
	[%]	3.90 % ± 0.2	3.70 % ± 0.2
a_s (AFM, $\overline{d_d}$)	[m^2/g]	108.00	96.00
a_s (AFM, $\overline{S_d}$)	[m^2/g]	110	100
a_s (N_2)[b]	[m^2/g]	112.00	102.00
a_s (EGME)[b]	[m^2/g]	737.00	755.00

[a] <2Na refer to the less or more than 2 μm Na-saturated size fraction.
[b] values are scaled to 100 % smectite content.

granulometric) grain size distribution compared to Calcigel (7.3 wt% and 2.2 wt% at $d = 0.063$ mm). This is attributed to the different production of the granulate (Section 1.1). Results of the separate sedimentation analyses reveal information about the actual intrinsic particle size distribution of the fine-grained material. The sedimentation of the <0.063 mm fraction of the granules shows that the particle size distributions of both bentonites are similar (solid lines). Contrary, the sedimentation of dispersed granules yields much higher fines content than of the <0.063 mm sieved fraction and Calcigel shows a finer intrinsic particle size distribution than Secursol UHP (dotted lines).

The geotechnical properties of the two bentonites revealed partly unexpected trends, which are discussed in terms of the different formation conditions of the natural materials (see Section 3.1) and their mineralogical composition. Despite its higher smectite content, higher a_s (N_2) (Table 1) and finer smectite particle sizes (Table 4), Secursol UHP has a 15–20 % lower liquid limit and approximately 25 % lower water uptake capacity than Calcigel. Further, Secursol UHP exhibits lesser dispersity of aggregates, which is also evident in the results of the sedimentation analysis using the raw granules (dotted lines in Fig. 8) and the size fractionation yields in this study which show that the <2 μm fraction in Secursol UHP is only 73 wt% compared to 98 wt% in Calcigel. The inherited rock structure of Secursol UHP (Section 3.1) reduces its plasticity and water uptake. The swelling index of Secursol UHP is, however, slightly higher than that of Calcigel, though similar in terms of measurement accuracy. Here, the higher smectite content and the non-evident carbonate content of Secursol UHP may outweigh the inherited structure, whose effect on dispersity otherwise prevails.

4. Summary and concluding remarks

In this study, the results of a comprehensive suite of characterization techniques that examine the mineralogy, physico-chemical and geotechnical properties are presented for two natural Ca/Mg bentonites from Germany. The bentonites Calcigel from Bavaria and Secursol UHP from Westerwald region are used in several laboratory and in-situ experiments in the context of underground nuclear waste repositories.

- Calcigel and Secursol UHP were confirmed to be Ca/Mg-bentonites with similar major mineralogical phases at different proportions. Both containing pure dioctahedral smectite phases. Secursol UHP has 20 % more smectite content.
- The smectite in Secursol UHP has about 45 % higher Ca: Mg ratio in comparison to Calcigel. It also exhibits higher layer charge, more Fe and less Al in its octahedral sheet, and slightly higher Mg (0.33 vs 0.31) resulting in a slightly higher specific density of smectite in Secursol UHP. From AFM data on single smectite layers, the average equivalent disc diameter is 25 % larger for Calcigel comparing to Secursol UHP with slightly higher average layer stacking in powder state of 9 layers vs 8 layer for Secursol UHP. While the latter shows a slightly wider smectite particle size distribution.
- For both bentonites, water content (of air-dry material) measured at 105°C is around 20 % (relative) lower than that measured at 200°C, suggesting the material remains partially in the first hydration state after drying at 105°C.
- Minor mineralogical phases content, particle morphology and size distribution results, and chemical composition of the smectite phase all indicate that Secursol UHP was formed under more stable physicochemical conditions compared to Calcigel. These findings are in line with the prevailing theories on the formation conditions of these

Table 5
Geotechnical characteristics of both bentonites and review of Calcigel geotechnical properties.

		This work		Literature (Calcigel)		
		Secursol UHP	Calcigel	Müller-Vonmoos and Kahr, 1983; Brenner, 1988	Samingan and Schanz, 2008	Baille et al., 2010; Schanz et al., 2018
Grain density (ρ_s)	[g/cm^3]	2.734	2.738	2.847[a]	2.65[a]	2.803[a]
Water content (w) 105°C	[wt%]	14.4	11.9	9.0	9.0–10.0	9.5
Ambient condition 200°C	[wt%]	18.6	14.6	–	–	–
Moisture (w_M) ambient condition 105°C	[wt%]	12.6	10.6	–	–	–
200°C	[wt%]	15.7	12.7	–	–	–
Liquid limit (w_L)	[%]	93[b] | 96[c]	117[b] | 110[c]	133 ± 3[b, c, e]	130[c]	178[c]
Plastic limit (w_p)	[%]	35	34	50	33	56
Shrinkage limit (w_S)	[%]	20	12	18	–	12
Plasticity Index (I_P)	[%]	58[b] | 61[c]	83[b] | 76[c]	80 ± 3	97	122
Consistency Index (I_c)	[%]	1.35 | 1.29[d]	1.27 | 1.23[d]	1.55	1.24	1.38
Smectite content	[wt%]	79	61	66	50–60	60

[a] Pycnometer method.
[b] Casagrande method.
[c] Fall cone method.
[d] Calculated as: $w_{105°C}$\| $w_{200°C}$: %.
[e] for a granular material 160 ± 9 was reported, but no further properties were stated.

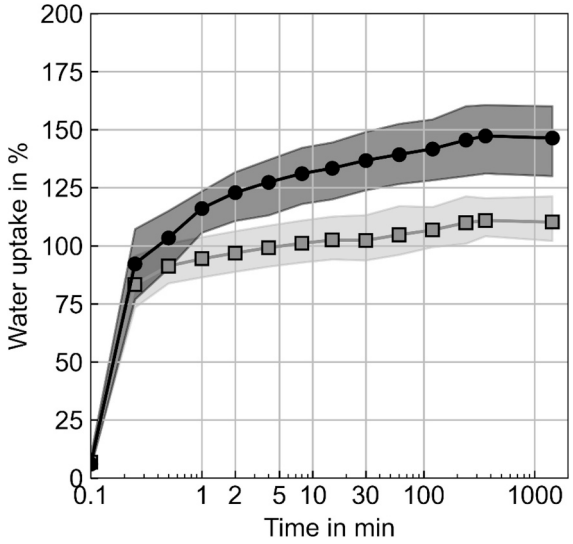

Fig. 7. Water uptake vs. time (Enslin-Neff) for Calcigel (black circles) and Securosol UHP (grey squares). The average value and a bandwidth of five tests is shown.

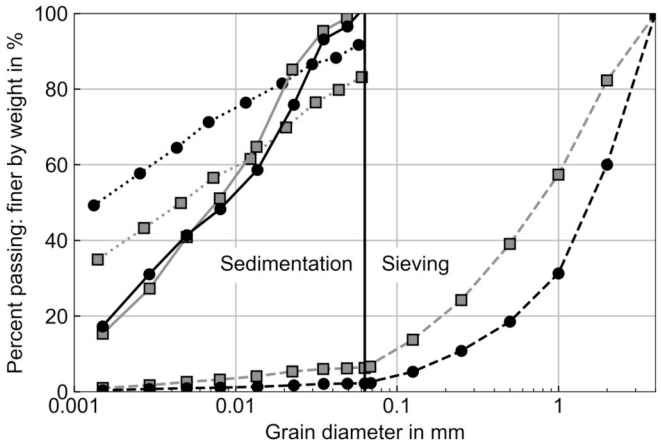

Fig. 8. Grain size distribution curve of granular Calcigel (black circles) and Securosol UHP (grey squares) from a combined sieve and sedimentation analysis (dashed line) and from sedimentation analysis of the <0.063 mm fine fraction (solid line) and of sedimentation of whole bentonite granules (dotted line).

two bentonites; Securosol UHP underwent in-situ bentonization process and was protected by an overlaying basalt layer. While Calcigel has been formed through alteration of acid vitreous tuff that was transported from other locations.

- The formation conditions likely helped Securosol UHP to preserve the fabric of its precursor, an assumption that could be also validated by SEM investigations cited in this work (Dohrmann, 2012). This inherited fabric, that apparently hinders smectite particle disaggregation and expansion upon hydration, was not completely destroyed during material pretreatment (section 1.2). Indeed, Securosol UHP yielded 25 wt% less <2 μm fraction than that of Calcigel, despite having 20 % higher smectite content and smaller particle size distribution (AFM, sieving and sedimentation tests). Moreover, the influence of this inherited fabric was clear in the results of the geotechnical classification performed on the granular materials without pretreatment. Calcigel clearly exhibits a 15–20 % higher liquid limit, 25 % greater water uptake, and better dispersibility in water, despite its lower smectite content, lower total surface area, and relatively coarser particle size compared to Securosol UHP. Although Securosol UHP shows a slightly higher swelling index than Calcigel, the difference remains within the margin of measurement accuracy.

Finally, the results of this work highlight the importance of comprehensive characterization of natural bentonite. General information, such as mineralogy, smectite content, and geotechnical limits, is insufficient to fully understand bentonite behavior, particularly upon hydration. Detailed approach analysis is crucial for predicting and optimizing the performance of bentonites in engineered barriers and sealing systems in landfills or underground repositories.

Declaration of generative AI and AI-assisted technologies in the writing process during the preparation of this work

The authors used Microsoft Copilot and DeepL in order to improve language and readability of the text (i.e., check grammar and punctuation). After using this tool, the authors reviewed and edited the content as needed and take full responsibility for the content of the publication.

CRediT authorship contribution statement

A. Asaad: Writing – review & editing, Writing – original draft, Visualization, Validation, Software, Methodology, Investigation, Formal analysis, Data curation, Conceptualization. **A. Nitsch:** Writing – review & editing, Writing – original draft, Visualization, Validation, Supervision, Software, Methodology, Investigation, Formal analysis, Data curation. **W. Baille:** Writing – review & editing, Validation, Supervision, Project administration, Investigation, Funding acquisition, Conceptualization. **K. Emmerich:** Writing – review & editing, Validation, Supervision, Project administration, Investigation, Funding acquisition, Conceptualization.

Funding

This research was funded by the German Federal Ministry for Economic Affairs and Energy (BMWi) under FKZ 02E12001 A + B. The project was managed by the Project management agency of Karlsruhe (PTKA).

Declaration of competing interest

The authors declare that they have no known competing financial interests or personal relationships that could have appeared to influence the work reported in this paper.

Acknowledgments

The authors are grateful to Ivo Herle, Heiner Siedel, Bernd Ullrich, and Reinhard Kleeberg (TU Bergakademie Freiberg) for retrieving very old conference proceedings on Lusatian bentonite, which could not be found in any database. We thank Eleanor Bakker (IMB-CMM, KIT) for the exchangeable cations' measurements and helpful discussions, Nadja Werling (IMB-CMM, KIT) for her assistance with STA measurements, Frank Heberling (INE, KIT) for his support with AFM measurements, and Jonas Kaltenbach (IFG, KIT) for his help with SEM analyses. We also acknowledge Annette Röthlisberger and Michael Plötze (ETH Zurich) for conducting the N_2 adsorption measurements, Peter Weidler (IFG, KIT) for water adsorption measurements, Nora Groschopf (Johannes Gutenberg University, Mainz) for XRF analyses, and R. Diedel (SSKG) for providing granular bentonites.

Finally, we sincerely thank the Editor and the two Reviewers of Applied Clay Science for their detailed reviews and constructive comments, which significantly contributed to improving the clarity and quality of our manuscript.

Appendix A. Supplementary data

Supplementary data to this article can be found online at https://doi.org/10.1016/j.clay.2025.107901.

Data availability

No data was used for the research described in the article.

References

Agus, S.S., Schanz, T., 2008. A method for predicting swelling pressure of compacted bentonites. Acta Geotech. 3, 125–137.

Allen, C.C., Wood, M.I., 1988. Bentonite in nuclear waste disposal: a review of research in support of the Basalt Waste Isolation Project. Appl. Clay Sci. 3, 11–30. https://doi.org/10.1016/0169-1317(88)90003-8.

Asaad, A., Hubert, F., Ferrage, E., Dabat, T., Paineau, E., Porion, P., Savoye, S., Gregoire, B., Dazas, B., Delville, A., Tertre, E., 2021. Role of interlayer porosity and particle organization in the diffusion of water in swelling clays. Appl. Clay Sci. 207, 106089. https://doi.org/10.1016/j.clay.2021.106089.

Asaad, A., Hubert, F., Dazas, B., Razafitianamaharavo, A., Brunet, J., Glaus, M.A., Savoye, S., Ferrage, E., Tertre, E., 2022. A baseline study of mineralogical and morphological properties of different size fractions of illite du Puy. Appl. Clay Sci. 224, 106517. https://doi.org/10.1016/j.clay.2022.106517.

Aziz, H.A., Böhme, M., Rocholl, A., Prieto, J., Wijbrans, J.R., Bachtadse, V., Ulbig, A., 2010. Integrated stratigraphy and 40 Ar/39 Ar chronology of the early to middle Miocene Upper Freshwater Molasse in western Bavaria (Germany). Int. J. Earth Sci. 99, 1859–1886.

Baille, W., Tripathy, S., Schanz, T., 2010. Swelling pressures and one-dimensional compressibility behaviour of bentonite at large pressures. Appl. Clay Sci. 48, 324–333. https://doi.org/10.1016/j.clay.2010.01.002.

Baille, W., Lang, L., Tripathy, S., Schanz, T., 2016. Influence of effective stress on swelling pressure of expansive soils. E3S Web Conf. 9, 14016. https://doi.org/10.1051/e3sconf/20160914016.

Bengtsson, A., Pedersen, K., 2017. Microbial sulphide-producing activity in water saturated Wyoming MX-80, Asha and Calcigel bentonites at wet densities from 1500 to 2000kgm−3. Appl. Clay Sci. 137, 203–212. https://doi.org/10.1016/j.clay.2016.12.024.

Bohác, P., Delavernhe, L., Zervas, E., Königer, F., Schuhmann, R., Emmerich, K., 2019. Cation exchange capacity of bentonite in a saline environment. Appl. Geochem. 100, 407–413. https://doi.org/10.1016/j.apgeochem.2018.12.019.

Bossart, P., Bernier, F., Birkholzer, J., Bruggeman, C., Connolly, P., Dewonck, S., Fukaya, M., Herfort, M., Jensen, M., Matray, J.-M., 2017. Mont Terri rock laboratory, 20 years of research: introduction, site characteristics and overview of experiments. Swiss J. Geosci. 110, 3–22. https://doi.org/10.1007/s00015-016-0236-1.

Bradley, W.F., Grim, R.E., Clark, G.L., 1937. A Study of the Behavior of Montmorillonite upon Wetting. Zeitschrift für Kristallographie - Crystalline Materials 97, 216–222. https://doi.org/10.1524/zkri.1937.97.1.216.

Brennecke, P.W., Kunze, V.H., 2000. Recent developments in the German approach to radioactive waste disposal. Radioactive waste management and decommissionin, WM'00 Conference, Tucson, AZ.

Brenner, R.P., January 1988. Bohrlochversiegelung: Materialeigenschaften von hochverdichtetem Bentonit mit Eignungsbeurteilung. Nagra Technischer Bericht 88–04. Elektrowatt Ingenieurunternehmung AG, Zürich.

Brindley, G.W., Brown, G., 1982. Crystal Structure of Clay Minerals and their X-Ray Identification, vol. 5. The Mineralogical Society of Great Britain and Ireland.

Brunauer, S., Emmett, P.H., Teller, E., 1938. Adsorption of gases in Multimolecular Layers. J. Am. Chem. Soc. 60, 309–319. https://doi.org/10.1021/ja01269a023.

Cadene, A., Durand-Vidal, S., Turq, P., Brendle, J., 2005. Study of individual Na-montmorillonite particles size, morphology, and apparent charge. J. Colloid Interface Sci. 285, 719–730. https://doi.org/10.1016/j.jcis.2004.12.016.

Carter, D.L., Heilman, M.D., Gonzales, C.L., 1965. Ethylene glycol monoethyl ether for determining surface area of silicate minerals. Soil Sci. 100, 356–360.

Cerato, A.B., Lutenegger, A.J., 2002. Determination of surface area of fine-grained soils by the ethylene glycol monoethyl ether (EGME) method. Geotech. Test. J. 25, 315–321.

Chiou, C.T., Rutherford, D.W., 1997. Effects of exchanged cation and layer charge on the sorption of water and EGME vapors on montmorillonite clays. Clay Clay Miner. 45, 867–880.

Deer, W.A., F, R.S., Howie, R.A., Zussman, J., 2013. An Introduction to the Rock-Forming Minerals. Mineral. Soc.Great Britain Ireland. https://doi.org/10.1180/DHZ.

Delage, P., Cui, Y.J., Tang, A.M., 2010. Clays in radioactive waste disposal. J. Rock Mech. Geotech. Eng. 2, 111–123. https://doi.org/10.3724/SP.J.1235.2010.00111.

Delavernhe, L., Steudel, A., Darbha, G.K., Schäfer, T., Schuhmann, R., Wöll, C., Geckeis, H., Emmerich, K., 2015. Influence of mineralogical and morphological properties on the cation exchange behavior of dioctahedral smectites. Colloids Surf. A Physicochem. Eng. Asp. 481, 591–599. https://doi.org/10.1016/j.colsurfa.2015.05.031.

Delay, J., Bossart, P., Ling, L.X., Blechschmidt, I., Ohlsson, M., Vinsot, A., Nussbaum, C., Maes, N., 2014. Three decades of underground research laboratories: what have we learned? Geol. Soc. Lond. Spec. Publ. 400, 7–32. https://doi.org/10.1144/SP400.1.

2020 DIN 18122-2:2020-11, 2020. Soil testing — Determination of the shrinkage limit of soils — Part 2: Laboratory method, 18122-2. Beuth Verlag, Berlin, pp. 2020–11.

DIN 18132, April 2012: Soil, testing procedures and testing equipment - Determination of water absorption.

DIN EN ISO 14688-2, November 2020. Geotechnical investigation and testing — Identification and classification of soil — part 2: Principles for a classification (ISO 14688-2:2017); German version EN ISO 14688–2, p. 2018.

DIN EN ISO 17892-1, March 2015. Geotechnical investigation and testing - Laboratory testing of soil - Part 1: Determination of water content (ISO 17892-1:2014 + Amd 1: 2022); German version EN ISO 17892-1:2014 + A1:2022.

DIN EN ISO 17892-12, July 2020. Geotechnical investigation and testing - Laboratory testing of soil - Part 12: Determination of liquid and plastic limits (ISO 17892-12: 2018 + Amd 1:2021 + Amd 2:2022); German version EN ISO 17892-12:2018 + A1: 2021 + A2:2022.

DIN EN ISO 17892-3, July 2016. Geotechnical investigation and testing - Laboratory testing of soil - part 3: Determination of particle density (ISO 17892-3:2015, Corrected version 2015-12-15). German version EN ISO 17892–17893, 2015.

DIN EN ISO 17892-4, April 2017. Geotechnical investigation and testing - Laboratory testing of soil - part 4: Determination of particle size distribution (ISO 17892-4: 2016). German version EN ISO 17892–17894, 2016.

Dixon, D.A., Birch, K., Stone, J., Kim, C.S., Barone, F., 2023. Measured swelling, hydraulic and thermal properties of MX-80 bentonite: Distinguishing between material variability and measurement limitations. Appl. Clay Sci. 241, 106998. https://doi.org/10.1016/j.clay.2023.106998.

Doebelin, N., Kleeberg, R., 2015. Profex: a graphical user interface for the Rietveld refinement program BGMN. J. Appl. Crystallogr. 48, 1573–1580. https://doi.org/10.1107/S1600576715014685.

Dohrmann, R., 2012. Tonmineralogie-Untersuchungen an einem Tongranulat für Kultursubstrate und dessen Ausgangsrohstoffen. Federal Institute for Geosciences and Natural Resources (BGR).

Drits, V.A., Zviagina, B.B., 2009. Trans-Vacant and cis-Vacant 2:1 Layer Silicates: Structural Features, Identification, and Occurrence. Clay Clay Miner. 57, 405–415. https://doi.org/10.1346/CCMN.2009.0570401.

Drits, V.A., Besson, G., Muller, F., 1995. An improved model for structural transformations of heat-treated aluminous dioctahedral 2: 1-layer silicates. Clay Clay Miner. 43, 718–731.

Emmerich, K., 2010. Thermal Analysis in the Characterization and Processing of Industrial Minerals. In: Ferraris, G., Christidis, G.E. (Eds.), Advances in the Characterization of Industrial Minerals. European Mineralogical Union, pp. 129–170. https://doi.org/10.1180/EMU-notes.9.5.

Emmerich, K., Smykatz-Kloss, W., 2002. Exothermic effects in soils during thermal analysis. Clay Miner. 37, 575–582. https://doi.org/10.1180/0009855023740060.

Emmerich, K., Kemper, G., Königer, F., Schlaeger, S., Gruner, M., Gaßner, W., Hofmann, M., Nüesch, R., Schuhmann, R., 2009a. Saturation Kinetics of a Vertical Multilayer Hydraulic Sealing System Exposed to Rock Salt Brine. Vadose Zone J. 8, 332–342. https://doi.org/10.2136/vzj2008.0094.

Emmerich, K., Wolters, F., Kahr, G., Lagaly, G., 2009b. Clay profiling: the classification of montmorillonites. Clay Clay Miner. 57, 104–114. https://doi.org/10.1346/CCMN.2009.0570110.

Emmerich, K., Giraudo, N., Schuhmann, R., Schnetzer, F., Kaden, H., Thissen, P., 2018. On the Prediction of Water Contents in Na-Saturated Dioctahedral Smectites. J. Phys. Chem. C 122, 7484–7493. https://doi.org/10.1021/acs.jpcc.7b11953.

Emmerich, K., Schuhmann, R., Königer, F., Bohac, P., Delavernhe, L., Wieczorek, K., Czaikowski, O., Hesser, J., Shao, H., Jaeggi, D., 2019. Joint project: Vertical hydraulic sealing system based on the Sandwich principle–preproject (Sandwich-VP). Final report. In: Karlsruher Institut für Technologie (KIT) & Gesellschaft für Anlagen-und Reaktorsicherheit (GRS) gGmbH.

Emmerich, K., Bakker, E., Königer, F., Rölke, C., Popp, T., Häußer, S., Diedel, R., Schuhmann, R., 2021. A MiniSandwich Experiment with Blended Ca-Bentonite and Pearson Water Hydration, Swelling. Solute Transport and Cation Exchange. Minerals 11, 1061. https://doi.org/10.3390/min11101061.

Ferrage, E., 2005. Investigation of smectite hydration properties by modeling experimental X-ray diffraction patterns: part I. Montmorillonite hydration properties. American Mineralogist 90, 1358–1374. https://doi.org/10.2138/am.2005.1776.

Ferrage, E., Lanson, B., Michot, L.J., Robert, J.-L., 2010. Hydration Properties and Interlayer Organization of Water and Ions in Synthetic Na-Smectite with Tetrahedral Layer Charge. Part 2. Toward a Precise Coupling between Molecular Simulations and Diffraction Data. J. Phys. Chem. C 114, 4515–4526. https://doi.org/10.1021/jp909860p.

Fontaine, F., Christidis, G.E., Yans, J., Hollanders, S., Hoffman, A., Fagel, N., 2020. Characterization and origin of two Fe-rich bentonites from Westerwald (Germany). Appl. Clay Sci. 187, 105444. https://doi.org/10.1016/j.clay.2020.105444.

Gilg, H.A., Ulbig, A., 2017. Bentonites, volcanogenic tonsteins and refractory clays in the Upper Freshwater Molasse and Paleo-Naab system. Bavaria. jber_oberrh 99, 191–214. https://doi.org/10.1127/jmogv/99/0006.

Greene-Kelly, R., 1957. The montmorillonite minerals (smectites). The differential thermal investigation of clays 2, 140.

Grim, R.E., Güven, N., 1978. Bentonites: geology, mineralogy, properties and uses, Developments in sedimentology. Elsevier Scientific Pub. Co.; distributors for the United States and Canada. Elsevier/North-Holland, Amsterdam; New York: New York.

Gruner, M., 2010. Utilization of Bentonite in Wase Disposal Mining. Einsatz von Bentonit im Entsorgungsbergbau, Bergbau (Hattingen), p. 61.

Herbert, H.-J., Moog, H.C., 2002. Untersuchungen zur Quellung von Bentoniten in hochsalinen Lösungen: Abschlußbericht. GRS, Köln Garching b. München Berlin Braunschweig, GRS.
Hlug, 2006. Hessisches Landesamt für Naturschutz, Umwelt und Geologie (TECHNICAL REPORT). Hessisches Landesamt für Umwelt und Geologie, Hessisches Ministerium für Umwelt, Umweltallianz Hessen.
Jalal, F.E., Xu, Y., Li, X., Jamhiri, B., Iqbal, M., 2021. Fractal approach in expansive clay-based materials with special focus on compacted GMZ bentonite in nuclear waste disposal: a systematic review. Environ. Sci. Pollut. Res. 28, 43287–43314. https://doi.org/10.1007/s11356-021-14707-7.
Kaufhold, S., Dohrmann, R., 2008. Comparison of the Traditional Enslin-Neff Method and the Modified Dieng Method for measuring Water-Uptake Capacity. Clay Clay Miner. 56, 686–692. https://doi.org/10.1346/CCMN.2008.0560609.
Kellomäki, A., Nieminen, P., Ritamäki, L., 1987. Sorption of ethylene glycol monoethyl ether (EGME). On homoionic montmorillonites. Clay Miner. 22, 297–303. https://doi.org/10.1180/claymin.1987.022.3.04.
Königer, F., Emmerich, K., Kemper, G., Gruner, M., Gaßner, W., Nüesch, R., Schuhmann, R., 2008. Moisture spreading in a multi-layer hydraulic sealing system (HTV-1). Eng. Geol. 98, 41–49. https://doi.org/10.1016/j.enggeo.2008.01.001.
Köster, H.M., 1977. Die Berechnung kristallchemischer Strukturformeln von 2:1-Schichtsilikaten unter Berücksichtigung der gemessenen Zwischenschichtladungen und Kationenumtauschkapazitäten, sowie die Darstellung der Ladungsverteilung in der Struktur mittels Dreieckskoordinaten. Clay Miner. 12, 45–54.
Köster, M.H., Hölzl, S., Gilg, H.A., 2017. A strontium isotope and trace element geochemical study of dolomite-bearing bentonite deposits in Bavaria (Germany). Clay Miner. 52, 161–190. https://doi.org/10.1180/claymin.2017.052.2.01.
Kugler, H., Ottner, F., Schwaighofer, B., Strasser, W., 2002. In: Ottner, H., Gier, S. (Eds.), Die Modifizierung des Wasseraufnahmeversuches nach Enslin-Neff. Berichte der DTTG, Vienna, Austria, p. 125À142.
Lagaly, G., 1981. Characterization of clays by organic compounds. Clay Miner. 16, 1–21. https://doi.org/10.1180/claymin.1981.016.1.01.
Lagaly, G., 1994. Layer charge determination by alkylammonium ions. In: Mermut, A.R., Boyd, S.A., Farmer, W.J., Jaynes, W.F., Lagaly, G., Laird, D.A., Mermut, A.R. (Eds.), Layer Charge Characteristics of 2:1 Silicate Clay Minerals. Clay Minerals Society, p. 0. https://doi.org/10.1346/CMS-WLS-6.1.
Landais, P., 2006. Advances in geochemical research for the underground disposal of high-level, long-lived radioactive waste in a clay formation. J. Geochem. Explor. 88, 32–36. https://doi.org/10.1016/j.gexplo.2005.08.011.
Lee, S.Y., Tank, R.W., 1985. Role of clays in the disposal of nuclear waste: a review. Appl. Clay Sci. 1, 145–162. https://doi.org/10.1016/0169-1317(85)90570-8.
Liu, H., Fu, T., Sarwar, M.T., Yang, H., 2023. Recent progress in radionuclides adsorption by bentonite-based materials as ideal adsorbents and buffer/backfill materials. Appl. Clay Sci. 232, 106796. https://doi.org/10.1016/j.clay.2022.106796.
Madsen, F.T., 1998. Clay mineralogical investigations related to nuclear waste disposal. Clay Miner. 33, 109–129. https://doi.org/10.1180/000985598545318.
Meier, L.P., Kahr, G., 1999. Determination of the cation exchange capacity (CEC) of clay minerals using the complexes of copper (II) ion with triethylenetetramine and tetraethylenepentamine. Clay Clay Miner. 47, 386–388.
Müller-Vonmoos, M., Kahr, G., 1983. Mineralogische untersuchungen von Wyoming bentonit MX-80 und Montigel. Technischer Bericht 83-12.
Nüesch, R., Brandelik, A., Hübner, C., Schuhmann, R., 2002. Verschlussstopfen und Verfahren zum Verschließen von untertägigen Hohlräumen. KIT, Karlsruhe.
Plaschke, M., Schäfer, T., Bundschuh, T., Ngo Manh, T., Knopp, R., Geckeis, H., Kim, J.I., 2001. Size Characterization of Bentonite Colloids by Different Methods. Anal. Chem. 73, 4338–4347. https://doi.org/10.1021/ac010116t.
Pusch, R., 1992. Use of bentonite for isolation of radioactive waste products. Clay Miner. 27, 353–361. https://doi.org/10.1180/claymin.1992.027.3.08.
Pusch, R., 2006. Chapter 11.4 clays and nuclear waste management. In: Developments in Clay Science. Elsevier, pp. 703–716. https://doi.org/10.1016/S1572-4352(05)01023-8.
Rawat, A., Lang, L., Baille, W., Dieudonne, A.-C., Collin, F., 2020. Coupled hydro-mechanical analysis of expansive soils: Parametric identification and calibration. J. Rock Mech. Geotech. Eng. 12, 620–629.
Samingan, A., Schanz, T., 2008. A method for predicting swelling pressure of compacted bentonites. Acta Geotechnica 3. https://doi.org/10.1007/s11440-008-0057-0, 125-13.
Schanz, T., Tripathy, S., Sridharan, A., 2018. Volume change behaviour of swelling and non-swelling clays upon inundation with water and a low dielectric constant fluid. Appl. Clay Sci. 158, 219–225. https://doi.org/10.1016/j.clay.2018.03.031.
Schuhmann, R., Emmerich, K., Kemper, G., Königer, F., 2009. Verschlusssystem mit Äquipotenzialsegmenten für die Untertägige Entsorgung (UTD und ELA) Gefährlicher Abfälle zur Sicherherstellung der Homogenen Befeuchtung der Dichtelemente und zur Verbesserung der Langzeitstabilität: Schlussbericht. Karlsruhe, Germany, Karlsruher Institut für Technologie.
Sellin, P., Leupin, O.X., 2013. The use of Clay as an Engineered Barrier in Radioactive-Waste Management, a review. Clay Clay Miner. 61, 477–498. https://doi.org/10.1346/CCMN.2013.0610601.
Smykatz-Kloss, W., 1974. Differential Thermal Analysis. Minerals and Rocks. Springer Berlin Heidelberg, Berlin, Heidelberg. https://doi.org/10.1007/978-3-642-65951-5.
Steudel, A., Emmerich, K., 2013. Strategies for the successful preparation of homoionic smectites. Appl. Clay Sci. 75–76, 13–21. https://doi.org/10.1016/j.clay.2013.03.002.
Svensson, D., Dueck, A., Nilsson, U., Olsson, S., Sandén, T., Lydmark, S., Jägerwall, S., Pedersen, K., Hansen, S., 2011. Alternative Buffer Material – Status of the Ongoing Laboratory Investigation of Reference Materials and Test Package 1 (Technical report No. SKB-TR-11-06).. LTH Lund University, Sweden.
Tournassat, C., Neaman, A., Villiéras, F., Bosbach, D., Charlet, L., 2003. Nanomorphology of montmorillonite particles: Estimation of the clay edge sorption site density by low-pressure gas adsorption and AFM observations. Am. Mineral. 88, 1989–1995. https://doi.org/10.2138/am-2003-11-1243.
Trümer, A., Ludwig, H.-M., Schellhorn, M., Diedel, R., 2019. Effect of a calcined Westerwald bentonite as supplementary cementitious material on the long-term performance of concrete. Appl. Clay Sci. 168, 36–42. https://doi.org/10.1016/j.clay.2018.10.015.
Tsipursky, S.I., Drits, V.A., 1984. The distribution of octahedral cations in the 2:1 layer of dioctahedral smectites studied by oblique-texture electron diffraction. Clay Miner. 19, 177–193. https://doi.org/10.1180/claymin.1984.019.2.05.
Ulbig, A., 1994. Vergleichende Untersuchungen an Bentoniten, Tuffen und sandig-tonigen Einschaltungen in den Bentonitlagerstätten der Oberen Süßwassermolasse Bayerns. TECHNISCHE UNIVERSITÄT MÜNCHEN, Munchin Germany.
Ulbig, A., 1999. Untersuchungen zur Entstehung der Bentonite in der bayerischen Oberen Süsswassermolasse. Neues Jahrbuch für Geologie und Paläontologie-Abhandlungen 214, 497–508.
Unger, H.J., Fiest, W., Niemeyer, A., 1990. Die Bentonite der ostbayerischen Molasse und ihre Beziehungen zu den Vulkaniten des Pannonischen Beckens. Geologisches Jahrbuch. Reihe D. 96, 67–112 (Mineralogie, Petrographie, Geochemie, Lagerstättenkunde.
Weidenthaler, C., 2011. Pitfalls in the characterization of nanoporous and nanosized materials. Nanoscale 3, 792. https://doi.org/10.1039/c0nr00561d.
Weinig, H., 1987. Bentonit (Bleicherde). Abb., 1 Foto. München 91, 135–142.
Wieczorek, K., Emmerich, K., Nagel, T., Bakker, E., Diedel, R., Furche, M., García-Siñeriz, J.L., Glaubach, U., Hesser, J., Hinze, M., Jaeggi, D., Königer, F., Mayor Zurdo, J.C., Räbiger, L., Rey Mazón, M., Rölke, C., Schädle, P., Schuhmann, R., Shao, H., Tuñón, S., Victoria Villar Galicia, M., Wilsnack, T., Yeatman, R., 2024. Sandwich-HP - Vertical Hydraulic Sandwich Sealing System- Final report. GRS-745.
Wieczorek, K., Emmerich, K., Schuhmann, R., Hesser, J., Furche, M., Jaeggi, D., Schefer, S., Aurich, J., Mayor, J.C., Norris, S., Birch, K., Sentis, M., García-Siñeriz, J. L., Königer, F., Glaubach, U., Rölke, C., Diedel, R., 2021. Large-scale testing of a sandwich shaft-sealing system at the Mont Terri rock laboratory. Saf. Nucl. Waste Disposal 1, 133–135. https://doi.org/10.5194/sand-1-133-2021.
Winston, P.W., Bates, D.H., 1960. Saturated Solutions for the Control of Humidity in Biological Research. Ecology 41, 232–237. https://doi.org/10.2307/1931961.
Wolters, F., Emmerich, K., 2007. Thermal reactions of smectites—Relation of dehydroxylation temperature to octahedral structure. Thermochim. Acta 462, 80–88. https://doi.org/10.1016/j.tca.2007.06.002.
Wolters, F., Lagaly, G., Kahr, G., Nueesch, R., Emmerich, K., 2009. A comprehensive characterization of dioctahedral smectites. Clay Clay Miner. 57, 115–133. https://doi.org/10.1346/CCMN.2009.0570111.